A deep learning-based model for automatic segmentation and evaluation of corneal neovascularization using slit-lamp anterior segment images

Xiaoran Chu[1][#][^], Xin Wang[2][#], Chen Zhang[1][^], Hui Liu[1], Fei Li[1], Guangxu Li[2,3][*], Shaozhen Zhao[1][*][^]

[1]Department of Cornea and Refractive Surgery, Tianjin Key Laboratory of Retinal Functions and Diseases, Tianjin Branch of National Clinical Research Center for Ocular Disease, Eye Institute and School of Optometry, Tianjin Medical University Eye Hospital, Tianjin, China; [2]School of Electronics and Information Engineering, Tiangong University, Tianjin, China; [3]Tianjin Optoelectronic Detection Technology and System Laboratory, Tianjin, China

Contributions: (I) Conception and design: X Chu; (II) Administrative support: S Zhao; (III) Provision of study materials or patients: C Zhang, H Liu; (IV) Collection and assembly of data: C Zhang, F Li, H Liu; (V) Data analysis and interpretation: X Chu, X Wang, G Li; (VI) Manuscript writing: All authors; (VII) Final approval of manuscript: All authors.

[#]These authors contributed equally to this work.

[*]These authors are co-corresponding authors.

Correspondence to: Shaozhen Zhao, MD, PhD. Department of Cornea and Refractive Surgery, Tianjin Key Laboratory of Retinal Functions and Diseases, Tianjin Branch of National Clinical Research Center for Ocular Disease, Eye Institute and School of Optometry, Tianjin Medical University Eye Hospital, 251 Fukang Road, Tianjin 300380, China. Email: szhao04@tmu.edu.cn; Guangxu Li, DE, PhD. School of Electronics and Information Engineering, Tiangong University, Tianjin 300387, China; Tianjin Optoelectronic Detection Technology and System Laboratory, 399 Binshui West Road, Tianjin 300387, China. Email: liguangxu@tiangong.edu.cn.

Background: Corneal neovascularization (CoNV) is a common sign in anterior segment eye diseases, the level of which can indicate condition changes. Current CoNV evaluation methods are time-consuming and some of them rely on equipment which is not widely available in hospitals. Thus, a fast and efficient evaluation method is now urgently required. In this study, a deep learning (DL)-based model was developed to automatically segment and evaluate CoNV using anterior segment images from a slit-lamp microscope.

Methods: A total of 80 cornea slit-lamp photographs (from 80 patients) with clinically manifested CoNV were collected from December 2021 to July 2022 at Tianjin Medical University Eye Hospital. Of these, 60 images were manually labelled by ophthalmologists using ImageJ software to train the vessel segmentation network IterNet. To evaluate the performance of this automated model, evaluation metrics including accuracy, precision, area under the receiver operating characteristic (ROC) curve (AUC), and F_1 score were calculated between the manually labelled ground truth and the automatic segmentations of CoNV of 20 anterior segment images. Furthermore, the vessels pixel count was automatically calculated and compared with the manually labelled results to evaluate clinical usability of the automated segmentation network.

Results: The IterNet model achieved an AUC of 0.989, accuracy of 0.988, sensitivity of 0.879, specificity of 0.993, area under precision-recall of 0.921, and F_1 score of 0.879. The Bland-Altman plot between manually labelled ground truth and automated segmentation results produced a concordance correlation coefficient of 0.989, 95% limits of agreement between 865.4 and −562.4, and the vessels pixel count's Pearson coefficient of correlation was 0.981 (P<0.01).

^ ORCID: Xiaoran Chu, 0000-0002-7875-9530; Chen Zhang, 0000-0001-9940-4205; Shaozhen Zhao, 0000-0001-7646-2699.

Conclusions: The fully automated network model IterNet provides a time-saving and efficient method to make a quantitative evaluation of CoNV using slit-lamp anterior segment images. This method demonstrates great value and clinical application potential for patient care and future research.

Introduction

The cornea is a transparent, avascular tissue located in the anterior of iris and pupil. Defects in any corneal layer (consisting of corneal epithelium, Bowman's layer, the corneal stroma, Descemet's membrane, and the corneal endothelium) will interrupt light entering the eye. Corneal neovascularization (CoNV), a clinical sign of abnormal vessels invading into the cornea and tipping the balance of angiogenic and antiangiogenic factors, is often accompanied with corneal opacity and contributes to varying degrees of visual decline (1).

CoNV resulting from limbal stem cell barrier damage occurs due to a wide variety of etiologies, including ocular inflammation, infection, trauma, chemical injury (e.g., alkali), ischemia, corneal graft rejection, congenital abnormalities, or systemic disorders such as Stevens-Johnson syndrome (2,3). It also can be categorized into superficial neovascularization, vascular pannus, and deep stromal vascularization according to the location of vessels (4). The existence of CoNV disrupts corneal relative immune privilege, and causes a positive feedback cycle of inflammation and increased vascularization (2). Thus, proliferation or regression of corneal neovessels is one of the most crucial aspects of disorder assessment and monitoring.

Clinical observation methods on CoNV range from slit-lamp bio-microscope photography, in vivo confocal microscopy (IVCM), and anterior segment optical coherence tomographic angiography (AS-OCTA) to corneal fluorescein angiography (FA) and indocyanine green angiography (ICGA). Manually circumscribing the blood vessel network with the cursor based on anterior segment slit-lamp photographs and then calculating the percentage of neovascularization area in the total corneal area can enable an initial quantitative evaluation of CoNV in a straightforward way (5,6), which is non-invasive and relatively simple to operate, but tracing vessels manually is laborious and easily affected by operator-subjective effects. IVCM is mainly used for describing the characteristics of CoNV such as red blood cell traffic and lymphatic vessels; the need for direct surface contact between the cornea and the microscope objective lens, limited view field, and long acquisition time are the limitations of its clinical use (7). FA and ICGA, the "gold standard" for detecting CoNV currently, can quantify vessels in a semiautomatic way and clearly distinguish afferent or efferent vessels (8,9), but rely relatively heavily on equipment and technicians. Moreover, dye intravenous injections can introduce certain serious adverse reactions such as potential anaphylaxis, meaning that patients with contraindications are unable to undergo these examinations (10,11). AS-OCTA is a good non-invasive, quantitative tool for objective CoNV assessment. The combination of en-face OCTA scan and cross-sectional plane provides multi-dimensional mapping and depth of corneal vessels; however, due to a limited image resolution with a small field of view, it may be inapplicable to evaluate the neovascularization of large areas (12-15).

In general, although there are various methods of CoNV detection, they are limited by hospital level and clinical technicians, besides, many patients are not willing to undergo invasive examinations such as angiography. Slit-lamps are commonly available in ophthalmology clinics, but although previous studies have shown that manually tracing vessels based on anterior slit-lamp images is an effective method to evaluate CoNV, it is time-consuming and volitional. Aiming to establish a non-invasive quantitative method and inspired by the application of highly accurate deep learning (DL) algorithms in ocular conditions [e.g., keratoconus (16), glaucoma diagnosis (17), dry eye disease (18), diabetic retinopathy (19), or corneal nerve evaluation (20,21)], we developed IterNet, a DL-based model that is trained on automatic segmentation and
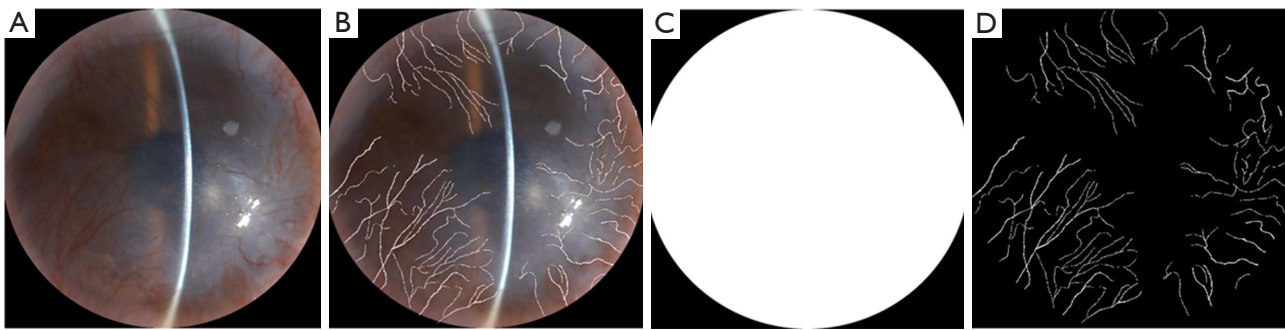
Figure 1 CoNV image annotation example. (A) Cropped original cornea image; (B) manually labeled annotated image; (C) mask image; (D) ground truth image without background. CoNV, corneal neovascularization.

evaluates different individuals' CoNV using slit-lamp anterior segment photographs, to extract and quantify corneal neovessels rapidly so as to assist ophthalmologists in disease condition assessment.

Methods

Data collection

To our knowledge, this is the first study to use a DL model to segment corneal vessels, and public datasets for this subject are absent, therefore, a private dataset was used in this study.

A total of 80 slit-lamp anterior segment images with CoNV were collected at Tianjin Medical University Eye Hospital from December 2021 to July 2022. The study was conducted in accordance with the Declaration of Helsinki (as revised in 2013). The study was approved by the Institutional Review Board of the Tianjin Medical University Eye Hospital [No. 2021KY(L)-53] and the requirement for individual consent for this retrospective analysis was waived. The images were taken with the digital camera (Topcon SL-D701; Topcon, Tokyo, Japan) attached to the slit-lamp, the illumination was set at a 45° angle from the display system during acquisition of all images, and magnification was set at 10 times to clarify the entire cornea. A clear picture captured from each eye was presented as 1 sample, pictures with obvious blur were excluded (see in the supplementary appendix online), and all pictures were saved in JPG format with 3,264×2,448 pixels without compression before being processed.

Image processing

All images were cropped first along the cornea limbus,

and were then resized into a valid area of 576×576 pixels. For algorithm development, the 80 images were randomly divided into a training set and a testing set containing 60 and 20 images, respectively. Visible corneal neovessels excluding blurred images of the training set images were labelled manually with a cursor by 2 independent ophthalmologists using Java-based ImageJ software (National Institutes of Health, Bethesda, MD, USA), and any discrepancy in the image labeling results was resolved by a simple majority vote with senior physicians. Based on the corresponding binary ground truth results, a calculation of CoNV area could be obtained by ImageJ software. Each sample in the training set included an original cornea image, manually labelled image, mask image, and ground truth result, as shown in *Figure 1*.

Architecture of DL-based model

In our experiment, we applied IterNet, which is based on U-Net with the additional ability to find obscured details of the vessel from actual segmented vessel images rather than raw input images. A previous reference noted that U-Net could extract the feature of vessels efficiently and has good performance in ocular fundus vessel segmentation (22,23). In order to make better use of well-extracted features from the U-Net model to infer the missing pieces in them, mini-U-Nets were added to the model architecture. In brief, mini-U-Nets were added after the base module U-Net for initial segmentation, where the input of each refinery module is the output of the second last layer of its preceding module, thus, the false vessel patterns exposed and the loss function of each vessel segmentation output can be fixed according to the correct labels during the process of training. Afterwards, the base module can consistently adjust
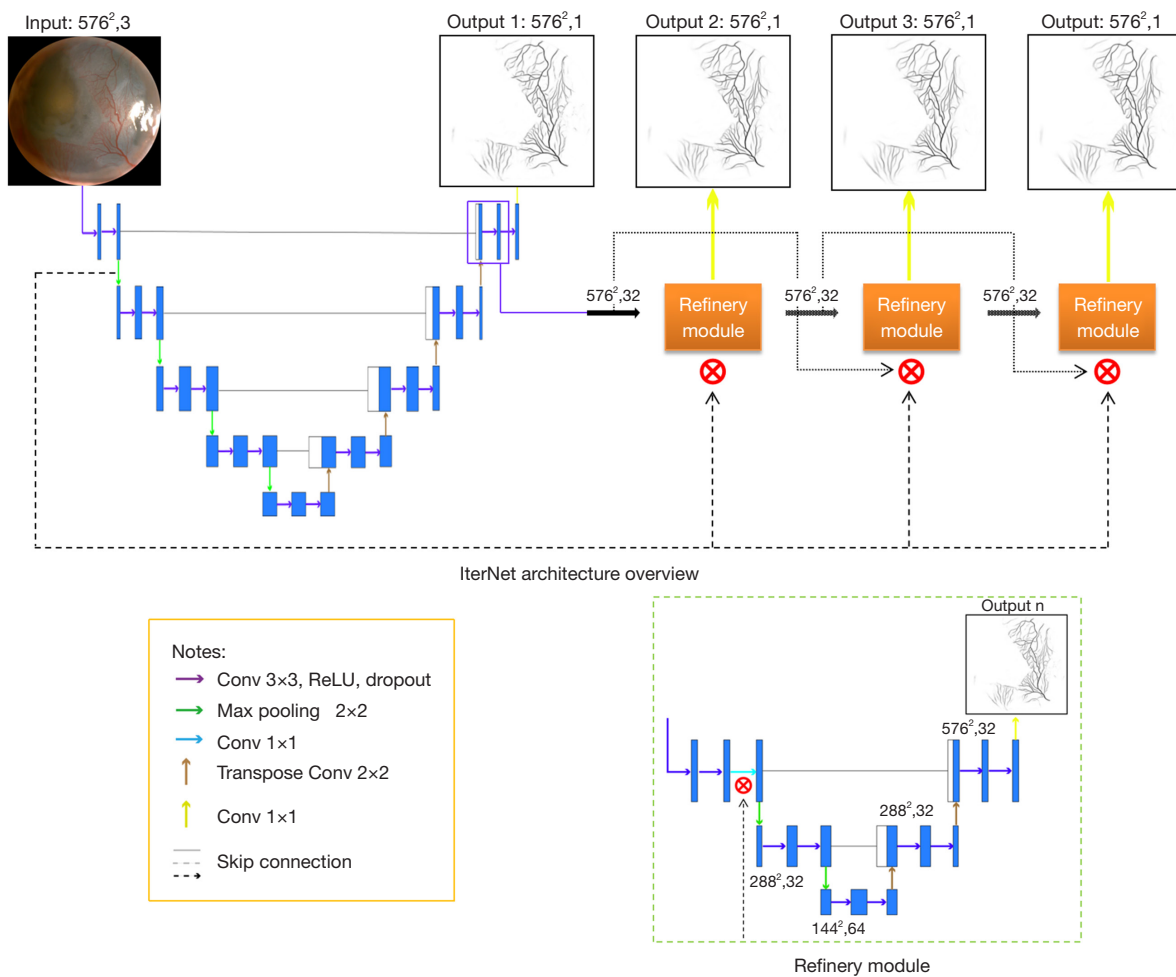
Figure 2 IterNet architecture overview: consists of 1 basic U-Net and 3 refinery modules (mini-U-Net). The size of final output is consistent with input in 576×576 pixels. ReLU, rectified linear unit; Conv, convolution.

parameters to improve output, and the vessels segmentation task can realize deeper than U-Net. Meanwhile, due to the skip-connection features of the architecture, IterNet can learn from 10–20 labelled images without prior training.

The structure of IterNet consists of 2 main architectures, as shown in *Figure 2*. One architecture is U-Net, a module based on the encoder-decoder idea, which has a total of 19 convolutional layers. The learning of the base module plays an important role in mapping from the original corneal images to the CoNV images. This helps to obtain a sketchy neovascularization segmentation map. The other architecture is mini-U-Net, which is a simplified version of U-Net consisting of 12 convolutional layers, the main responsibility of which is to process details such as micro-vessels, branches, or terminal backbones of vessels. Mini U-Net is applied iteratively in this network, the number of

iterations is set to 3, and it contributes a better completion of the false vessels correction. The output of the third mini-U-Net is recognized as the final output of this network.

As the model deepens in this process, the problem of gradient disappearance is unavoidable. To address this problem, a path from the upper layer to the lower layer is added in the network to obtain an efficient back-propagation. Thus, IterNet has three kinds of skip connections. The first is an intra-module connection, which serves to connect the encoding and decoding layers of each module. This connection introduces the feature information of the coding layer on the corresponding scale into the upsampling process, which has a higher feature resolution, thus, more accurate segmentation results can be obtained. The second is the connection from the base module to the refinery modules, it is an access of feature acquisition

6782

Chu et al. IterNet model for CoNV segmentation

Table 1 Experimental software and hardware environment configuration

Hardware environment
CPU: Intel(R) Xeon(R)Gold 5118
GPU: Tesla P100-PCIE-16GB
Software environment
Operating system: Ubuntu 20.04.4 LTS
Deep learning framework: Tensorflow 1.15.0
Development language: Python
Dependencies: Opencv, Numpy, etc.

CPU, central processing unit; GPU, graphics processing unit.

from the first layer of the base U-Net, which is very closely approximating the original corneal image. The feature is linked with the feature from each refinery module's first layer. The third is the connection among refinery modules, which concatenates the features of the lower modules to the upper modules.

Owing to 1 anterior segment photograph representing each sample, the total number of images we collected was limited. Meanwhile, IterNet can be seen as the same module running in a single forward path multiple times. In order to meet demand with possible variations such as color, shape, and position of vessels, data augmentation is essential to adapt the model to different environments, color ranges, and so on. Thus, we used extracted image patches with the size of 128 pixels to train the network to avoid overfitting during the training process.

The experimental platform is Tesla P100-PCIE-16GB graphics processing unit (GPU), and relies on the Tensorflow framework and Keras implementation. The training process is based on Python 3.7.6 (Python Software Foundation, Wilmington, DE, USA) and uses Adam optimizer; the batch size is set to 32, learning rate is 0.001, and the epoch is 300. The detailed configuration environment is listed in *Table 1*.

Evaluation metrics

To objectively and quantitatively evaluate the performance of IterNet, we conducted comparison on the network segmentation results and the manually labelled ground truth images by ophthalmologists from the aspects of accuracy, sensitivity, and specificity. The metrics were calculated as follows. First, we used 4 cases to evaluate the IterNet

segmentation results of each pixel: (I) true positive (TP) indicates that a real vessel point is predicted as a vessel point in the network system; (II) true negative (TN) indicates that a background point is predicted belong to background; (III) false positive (FP) indicates a real background point is mistakenly predicted as a vessel point; (IV) false negative (FN) indicates that the vessel point is predicted as a background point. Then, based on above pixel-level results, the system calculated accuracy, sensitivity, specificity, and precision metrics. In our study, accuracy was defined as the percentage of pixel points the network correctly predicted in overall image pixel points, and precision was the percentage of true vessel pixel points in proportion to the whole vessel pixel points; sensitivity and specificity indicated the result of true vessel or background pixel points that were precisely predicted by IterNet, respectively. The *F* score is a comprehensive evaluation value equivalent to the harmonic mean function of precision and recall (sensitivity is generally represented as "recall" during *F* score calculation), it will be close to 1 (the maximum value, $F \in [0, 1]$) only when these 2 are both high. The definitions of the above evaluation indicators are as follows (β value is set to 1):

$$\text{Accuracy} = \frac{TP + TN}{TP + FP + TN + FN} \quad [1]$$

$$\text{Specificity} = \frac{TN}{TN + FP} \quad [2]$$

$$\text{Sensitivity} = \frac{TP}{TP + FN} \quad [3]$$

$$\text{Precision} = \frac{TP}{TP + FP} \quad [4]$$

$$F_\beta = \left(1 + \beta^2\right) \frac{\text{Precision} * \text{Recall}}{\beta^2 * \left(\text{Precision} + \text{Recall}\right)} \quad [5]$$

Dice coefficient was used to measure the similarity between the network segmentation result and the ground truth, according to the following definition:

$$\text{Dice} = \frac{2 * TP}{\left(TP + FN\right) + \left(TP + FP\right)} \quad [6]$$

During model training, loss functions of each output (Out *n*) were defined as follows:

$$L_n = -y_n \log\left(p_n\right) - \left(1 - y_n\right) \log\left(1 - p_n\right) \quad [7]$$

where y_n ($y_n \in [0, 1]$) represents whether the ground truth for the label is correct for the pixel *n*, and p_n is the predicted
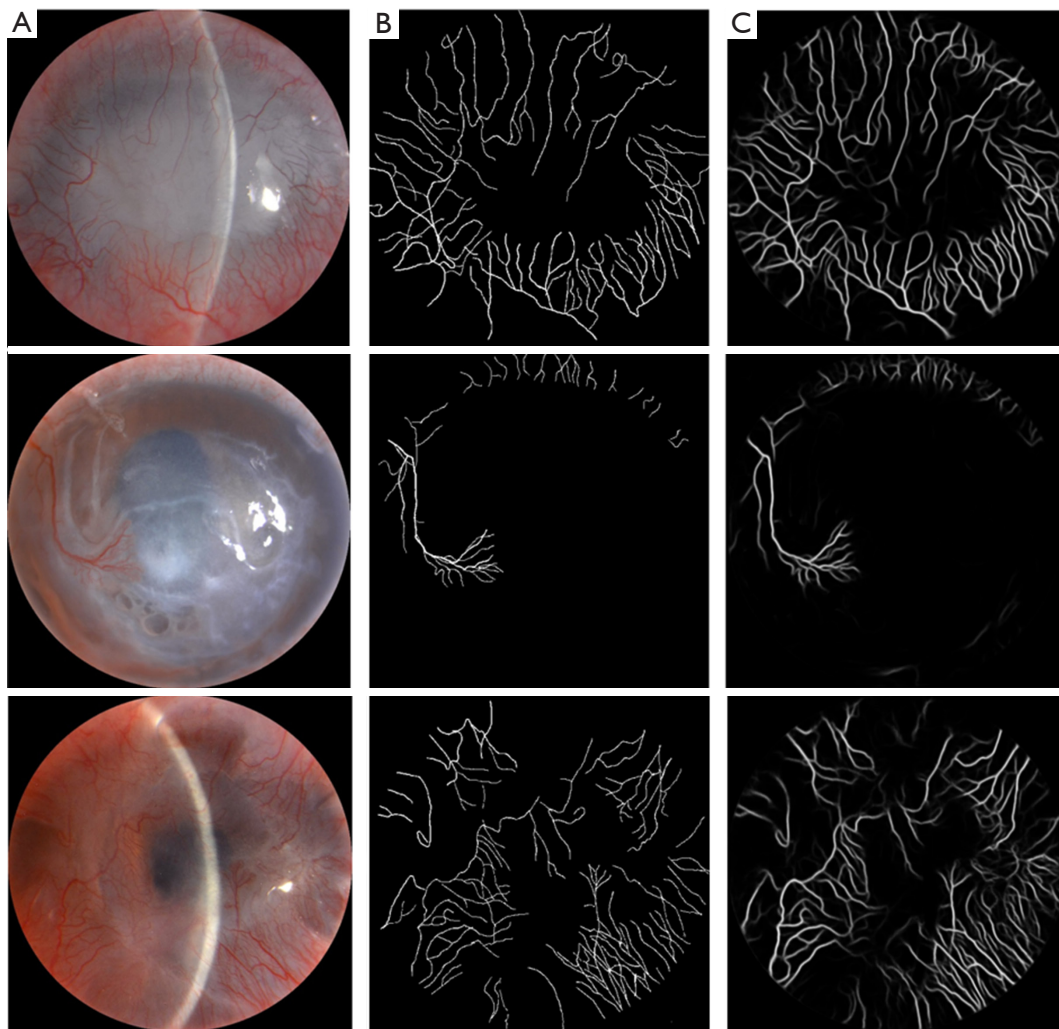
Figure 3 Examples of CoNV segmentation by IterNet. The images in the first column are input images (A); the second column shows images with manually traced corneal vessels (B); and the final column are images from the output of the segmentation network (C). CoNV, corneal neovascularization.

probability that the pixel n is a vessel pixel. The total loss functions value is the sum of each output.

We logged the total pixels count of vessels from manually-labelled ground truth images and automatically segmented images, regarded as the morphometric parameter and used for further comparison analysis and calculation.

Statistical analysis

The software packages SPSS version 22.0 (IBM Corp., Armonk, NY, USA) and MedCalc version 19.0.4 (MedCalc Software, Ostend, Belgium) were used for statistical analysis. The agreement between the automated segmentation results and the manually labelled work was evaluated using Bland-Altman plot. The correlation between the manually labelled vessels pixel count and the IterNet segmented vessels pixel count was assessed by Pearson's test. The receiver operating characteristic (ROC) curve and the precision-recall curve were performed with Python version 3.7.6. A 2-tailed P value <0.05 was considered statistically significant.

Results

As illustrated in *Figure 3*, the automated segmentation network extracted visible corneal vessels to a relatively large degree, and showed morphological variation of
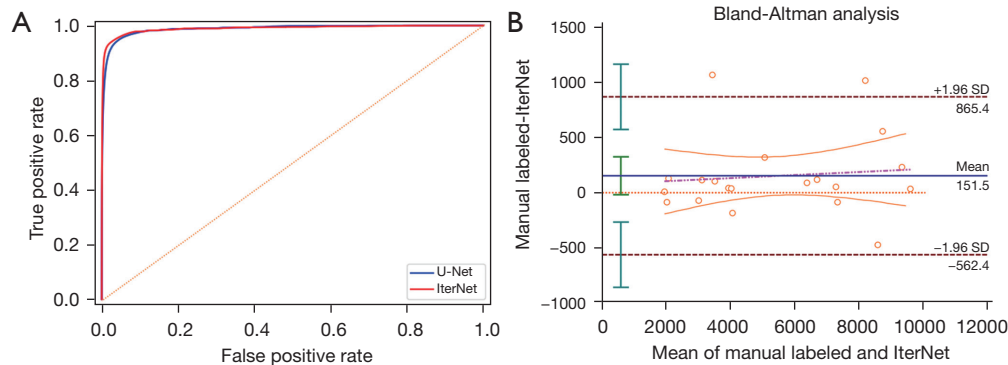
6784

Chu et al. IterNet model for CoNV segmentation

Figure 4 Performance evaluation of IterNet. (A) The ROC curve of IterNet and U-Net models. The AUC of IterNet and U-Net is 0.989 and 0.987, respectively. (B) Bland-Altman plots for comparing the pixels counts of manually labeled vessels and IterNet segmented vessels for the testing set, showing a good coherence between manual work and automated segmentation result. SD, standard deviation; ROC, receiver operating characteristic; AUC, area under the ROC curve.

Table 2 The comparison of segmentation results between IterNet and U-Net

Model	AUC	Accuracy	Sensitivity	Specificity	Dice coefficient	Precision	F_1 score
IterNet	0.989	0.988	0.879	0.993	0.879	0.878	0.879
U-Net	0.987	0.981	0.859	0.987	0.815	0.775	0.815

AUC, area under the receiver operator characteristic curve.

vessels which are consistent with the original morphology compared with manually labelled vessels.

To specifically evaluate IterNet performance, the ROC curve of the CoNV segmentation network result on the testing set was illustrated (*Figure 4A*), and as can be seen from the curves, the area under the IterNet ROC is larger than U-Net ROC. The other evaluation metrics of IterNet including sensitivity, specificity, accuracy, precision, and Dice coefficient were higher than those of U-Net, as shown in *Table 2*. Besides, the areas under precision-recall curves of IterNet and U-Net were 0.921 and 0.889, respectively.

The Bland-Altman plot for evaluating the consistency between IterNet segmentation results and the ground truth is presented in *Figure 4B*, and the 95% agreement limits between them are between 865.4 and –562.4 [concordance correlation coefficient (CCC) =0.989]. The Pearson's correlation coefficient of pixel count between manually labelled vessels and IterNet segmented vessels was 0.981 [95% confidence interval (CI): 0.976–0.996, P<0.01].

Based on the above analysis results, after all the images has been processed in a normalization method (cropped images were resized into a valid size pixels), the percentage of automated segmentation vessels pixel count in proportion

to the whole mask image can be used for condition assessment and therapy monitoring, resembling an "area" ratio. For example, as shown in *Figure 5*, the images of a patient with CoNV were analyzed via IterNet: the percentage of vessels that had invaded into the cornea had fallen from 4.766% (12,206 pixels) to 0.801% (2,052 pixels) after treatment, denoting the therapeutic effect quantitatively, accordingly, 5.012% (12,837 pixels) reduced to 0.768% (1,967 pixels) in manually labelled images, which indicates a minor difference of value difference between automatic segmentation and manual work.

Discussion

In this study, we described a fully automated method for the objective segmentation of corneal neovessels using slit-lamp anterior segment images. The automatic segmentation results showed a high agreement with the manually labelled ground truth performed by ophthalmologists, and the morphometric parameter calculation of segmented vessels pixels count realized a quantitative description of CoNV, which could be used for comparative studies in the future.

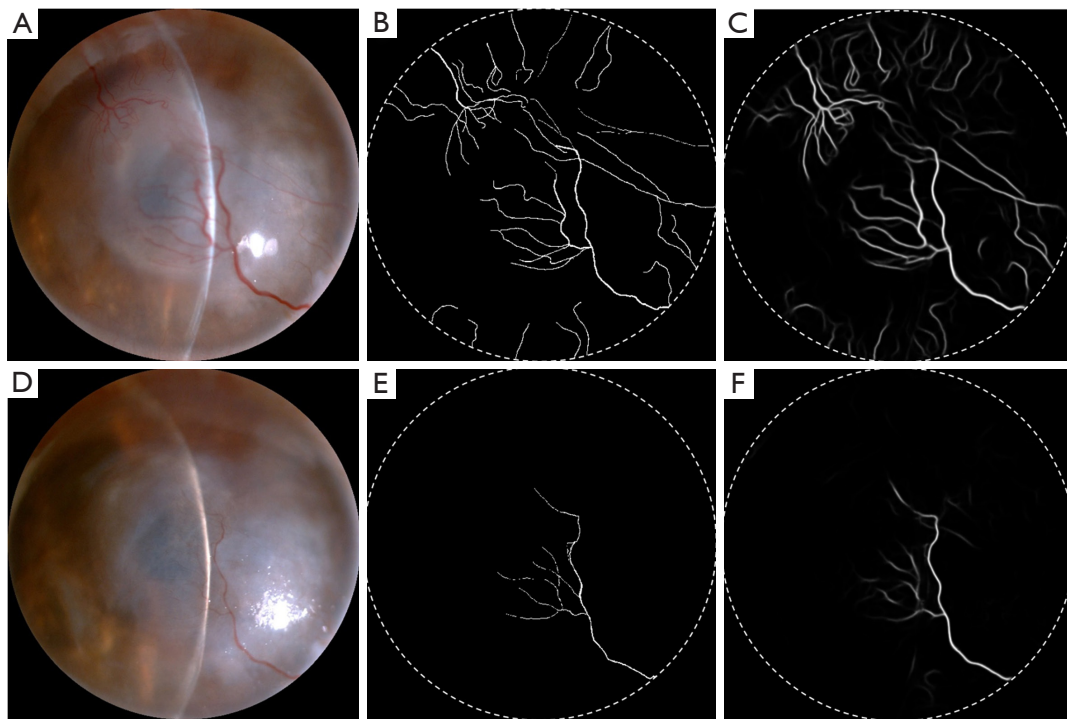A literature review of previous studies revealed that the

Figure 5 An example of CoNV regression after treatment. The images in the upper (A-C) and lower (D-F) rows illustrate conditions pre- and post-treatment, respectively (B,E: manually labelled annotation; C,F: IterNet segmentation). Circles in dotted lines represent the range of the whole cornea. CoNV, corneal neovascularization.

quantitative analysis of CoNV included a semiquantitative method and a semiautomatic method. Lai et al. classified corneal angiogenesis into 4 grade scales dependent on the numbers of vessels of the entire cornea (0, no vertical vessel; I, 1–6 vessels; II, 7–15 vessels; III, more than 15 vessels), which was regarded as an indicator of therapeutic effect in the study (24). Obviously, it was not sufficient enough when the area or length of vessels changed rather than numbers. Other semiquantitative methods such as dividing cornea into several quadrants and assessing vessels with scores according to the density or extent beyond the limbus face the same problem (25-27). Some researchers tend to apply the method of staining corneas with anti-CD31/PECAM-1 (the typical blood vessel molecular marker) antibody and fluorescein-conjugated secondary antibody, then observe and evaluate corneal vessels by the image analysis program Cell^F (Olympus Soft Imaging Solutions GmbH, Münster, Germany) (28-30), which is a comprehensive semiautomatic method but only available in animal experiments. In clinical practice, the combined use of imaging systems (FA, ICGA, or AS-OCTA) and image editing software such as ImageJ or Enhance is appealing; however, it is worth noting that

the fluorescein sodium leakage may affect vessel observation and assessment, and AS-OCTA may produce artifacts which are recognized as abnormal vessels (15,31,32). Compared with the aforementioned approaches, the automated segmentation model IterNet using slit-lamp images can avoid invasive operation and obtain a relatively thorough evaluation of vessels in the whole cornea.

Manual vessel tracing based on color images is not unusual in studies (5,6,33). Dastjerdi et al. proposed a computer-assisted method using Photoshop (Adobe, San Jose, CA, USA) to trace vessels and a written MATLAB program (MathWorks, Natick, MA, USA) to calculate corneal neovessel parameters (34), but the tracing work is time-consuming and low in repeatability due to the fact that manual operation by ophthalmologists may produce different performances in different situations. In comparison, the IterNet model performed vessel extraction repeatedly and achieved stable and consistent results. It was estimated that the developed network system takes less than 2 minutes to accomplish vessel segmentation and morphometric parameter quantification with the process on a GPU, which reduces time sharply and shows great

6786

Chu et al. IterNet model for CoNV segmentation

potential value of application in assisting clinical practice.

There were several limitations to our study. First, the results of IterNet performance evaluation indicate that the algorithm produced a relatively low sensitivity and precision for corneal neovessel segmentation compared with manually labelled results. In similarity with AS-OCTA, of which the results may not include the vessels with minimal flow or blocked signal from corneal opacities (13,35), vessels located in the deep stromal layer or covered by opacities were indistinguishable in slit-lamp images and hard to be outlined accurately. Although we manually labelled as many vessels as possible, the results were still less exhaustive than those of FA or ICGA, and the algorithm was prone to mistake vague vessels for false patterns and fix them. Second, because the cornea is not a horizontal plane, any anterior segment photographs taken may be influenced by illumination position or low contrast, which means that not all the vessels are captured clearly and increases difficulty in segmentation, especially in serious cases with CoNV. Therefore, the quality of images acquired for model processing needs to be guaranteed, and those with poor quality may produce a decrease in performance of the model in real-world practice. In a recent research on retinal vessel segmentation, a method was proposed based on the multi-scale retinex algorithm and multi-scale Gaussian-matched filtering method, showing more small blood vessels and better integrity of vascular structure, which may help to improve image processing to compensate for image quality (36). This might be a possible solution to improve slit-lamp images.

We recognize the limitations of our preliminary study. It would have been more comprehensive to be evaluated by a prospective study of CoNV with comparisons with angiography techniques or AS-OCTA. Nevertheless, this is still an innovative attempt to apply a DL-based model in corneal vessel segmentation and evaluation, demonstrating a great performance and the potential to aid in further making a quantitative estimation of abnormal neovessels in various corneal diseases.

What is more interesting is that corneal neovessels evaluation may be actualized at local clinics or even at home. Previous studies have shown that smartphones with camera attachments can capture ocular fundus images for screening and monitoring fundus lesions such as diabetic retinopathy (37,38). Inspired by which, patients with corneal disorders may undergo an initial assessment by means of IterNet, dependent only on the requirement of a clear and complete corneal picture. The combination of artificial intelligence (AI) and modern technologies will greatly improve health self-management, and we believe this advancement will be necessary for the large aging population in the near future.

Conclusions

Based on slit-lamp anterior segment images, we presented a fully automatic method for segmenting corneal neovessels and evaluating their quantitative parameters, which shows good performance. Compared to existing CoNV assessment methods, IterNet realized a combination of accuracy and efficiency, and is a novel application of computer-aided diagnosis. In addition, the equipment required is commonly available, and the entire process is noninvasive; it is also a breakthrough in the management of corneal diseases. Further validation of the IterNet model in a larger population in a clinical setting is required, and it is necessary to compare it with other imaging techniques. Further research is required to validate the potential of the model to improve the management of patients with CoNV.

Acknowledgments

Footnote

Conflicts of Interest: All authors have completed the ICMJE uniform disclosure form (available at https://qims.amegroups.com/article/view/10.21037/qims-23-99/coif). The authors have no conflicts of interest to declare.

Ethical Statement: The authors are accountable for all aspects of the work in ensuring that questions related to the accuracy or integrity of any part of the work are appropriately investigated and resolved. The study was conducted in accordance with the Declaration of Helsinki (as revised in 2013). The study was approved by the Institutional Review Board of the Tianjin Medical University Eye Hospital [IRB No. 2021KY(L)-53] and the requirement for individual consent for this retrospective analysis was waived.

Open Access Statement: This is an Open Access article distributed in accordance with the Creative Commons

Attribution-NonCommercial-NoDerivs 4.0 International License (CC BY-NC-ND 4.0), which permits the non-commercial replication and distribution of the article with the strict proviso that no changes or edits are made and the original work is properly cited (including links to both the formal publication through the relevant DOI and the license). See: https://creativecommons.org/licenses/by-nc-nd/4.0/.

References

1. Beebe DC. Maintaining transparency: a review of the developmental physiology and pathophysiology of two avascular tissues. Semin Cell Dev Biol 2008;19:125-33.

2. Nicholas MP, Mysore N. Corneal neovascularization. Exp Eye Res 2021;202:108363.

3. Abdelfattah NS, Amgad M, Zayed AA, Salem H, Elkhanany AE, Hussein H, Abd El-Baky N. Clinical correlates of common corneal neovascular diseases: a literature review. Int J Ophthalmol 2015;8:182-93.

4. Sharif Z, Sharif W. Corneal neovascularization: updates on pathophysiology, investigations & management. Rom J Ophthalmol 2019;63:15-22.

5. Wu PC, Liu CC, Chen CH, Kou HK, Shen SC, Lu CY, Chou WY, Sung MT, Yang LC. Inhibition of experimental angiogenesis of cornea by somatostatin. Graefes Arch Clin Exp Ophthalmol 2003;241:63-9.

6. Cursiefen C, Cao J, Chen L, Liu Y, Maruyama K, Jackson D, Kruse FE, Wiegand SJ, Dana MR, Streilein JW. Inhibition of hemangiogenesis and lymphangiogenesis after normal-risk corneal transplantation by neutralizing VEGF promotes graft survival. Invest Ophthalmol Vis Sci 2004;45:2666-73.

7. Romano V, Steger B, Zheng Y, Ahmad S, Willoughby CE, Kaye SB. Angiographic and In Vivo Confocal Microscopic Characterization of Human Corneal Blood and Presumed Lymphatic Neovascularization: A Pilot Study. Cornea 2015;34:1459-65.

8. Ang M, Cai Y, MacPhee B, Sim DA, Keane PA, Sng CC, Egan CA, Tufail A, Larkin DF, Wilkins MR. Optical coherence tomography angiography and indocyanine green angiography for corneal vascularisation. Br J Ophthalmol 2016;100:1557-63.

9. Kirwan RP, Zheng Y, Tey A, Anijeet D, Sueke H, Kaye SB. Quantifying changes in corneal neovascularization using fluorescein and indocyanine green angiography. Am J Ophthalmol 2012;154:850-858.e2.

10. Kwiterovich KA, Maguire MG, Murphy RP, Schachat AP, Bressler NM, Bressler SB, Fine SL. Frequency of adverse systemic reactions after fluorescein angiography. Results of a prospective study. Ophthalmology 1991;98:1139-42.

11. Stanga PE, Lim JI, Hamilton P. Indocyanine green angiography in chorioretinal diseases: indications and interpretation: an evidence-based update. Ophthalmology 2003;110:15-21; quiz 22-3.

12. Foo VHX, Ke M, Tan CQL, Schmetterer L, Mehta JS, Ang M. Anterior Segment Optical Coherence Tomography Angiography Assessment of Corneal Vascularisation After Combined Fine-Needle Diathermy with Subconjunctival Ranibizumab: A Pilot Study. Adv Ther 2021;38:4333-43.

13. Ang M, Cai Y, Shahipasand S, Sim DA, Keane PA, Sng CC, Egan CA, Tufail A, Wilkins MR. En face optical coherence tomography angiography for corneal neovascularisation. Br J Ophthalmol 2016;100:616-21.

14. Chan SY, Pan CT, Feng Y. Localization of Corneal Neovascularization Using Optical Coherence Tomography Angiography. Cornea 2019;38:888-95.

15. Cursiefen C, Viaud E, Bock F, Geudelin B, Ferry A, Kadlecová P, et al. Aganirsen antisense oligonucleotide eye drops inhibit keratitis-induced corneal neovascularization and reduce need for transplantation: the I-CAN study. Ophthalmology 2014;121:1683-92.

16. Kovács I, Miháltz K, Kránitz K, Juhász É, Takács Á, Dienes L, Gergely R, Nagy ZZ. Accuracy of machine learning classifiers using bilateral data from a Scheimpflug camera for identifying eyes with preclinical signs of keratoconus. J Cataract Refract Surg 2016;42:275-83.

17. Phene S, Dunn RC, Hammel N, Liu Y, Krause J, Kitade N, Schaekermann M, Sayres R, Wu DJ, Bora A, Semturs C, Misra A, Huang AE, Spitze A, Medeiros FA, Maa AY, Gandhi M, Corrado GS, Peng L, Webster DR. Deep Learning and Glaucoma Specialists: The Relative Importance of Optic Disc Features to Predict Glaucoma Referral in Fundus Photographs. Ophthalmology 2019;126:1627-39.

18. Xiao P, Luo Z, Deng Y, Wang G, Yuan J. An automated and multiparametric algorithm for objective analysis of meibography images. Quant Imaging Med Surg 2021;11:1586-99.

19. Lee PK, Ra H, Baek J. Automated segmentation of ultra-widefield fluorescein angiography of diabetic retinopathy using deep learning. Br J Ophthalmol 2022. [Epub ahead of print]. doi: 10.1136/bjo-2022-321063.

20. Wei S, Shi F, Wang Y, Chou Y, Li X. A Deep Learning Model for Automated Sub-Basal Corneal Nerve Segmentation and Evaluation Using In Vivo Confocal Microscopy. Transl Vis Sci Technol 2020;9:32.

21. Li G, Li T, Li F, Zhang C. NerveStitcher: Corneal confocal microscope images stitching with neural networks. Comput Biol Med 2022;151:106303.

22. Li L, Verma M, Nakashima Y, Nagahara H, Kawasaki R. IterNet: Retinal Image Segmentation Utilizing Structural Redundancy in Vessel Networks. 2020 IEEE Winter Conference on Applications of Computer Vision (WACV); 01-05 March 2020; Snowmass, CO, USA. IEEE; 2020:3645-54.

23. Ronneberger O, Fischer P, Brox T. U-Net: Convolutional Networks for Biomedical Image Segmentation. In: Navab N, Hornegger J, Wells W, Frangi A. editors. Medical Image Computing and Computer-Assisted Intervention – MICCAI 2015. Lecture Notes in Computer Science, vol 9351. Springer, Cham; 2015:234-41.

24. Lai LJ, Xiao X, Wu JH. Inhibition of corneal neovascularization with endostatin delivered by adeno-associated viral (AAV) vector in a mouse corneal injury model. J Biomed Sci 2007;14:313-22.

25. Cursiefen C, Wenkel H, Martus P, Langenbucher A, Nguyen NX, Seitz B, Küchle M, Naumann GO. Impact of short-term versus long-term topical steroids on corneal neovascularization after non-high-risk keratoplasty. Graefes Arch Clin Exp Ophthalmol 2001;239:514-21.

26. Ko BY, Kim YS, Baek SG, Lee GW, Kim JM, Jean WS, Lee NS, Kang J. Inhibition of corneal neovascularization by subconjunctival and topical bevacizumab and sunitinib in a rabbit model. Cornea 2013;32:689-95.

27. Pérez-Santonja JJ, Campos-Mollo E, Lledó-Riquelme M, Javaloy J, Alió JL. Inhibition of corneal neovascularization by topical bevacizumab (Anti-VEGF) and Sunitinib (Anti-VEGF and Anti-PDGF) in an animal model. Am J Ophthalmol 2010;150:519-528.e1.

28. Bock F, Onderka J, Hos D, Horn F, Martus P, Cursiefen C. Improved semiautomatic method for morphometry of angiogenesis and lymphangiogenesis in corneal flatmounts. Exp Eye Res 2008;87:462-70.

29. Dietrich T, Onderka J, Bock F, Kruse FE, Vossmeyer D, Stragies R, Zahn G, Cursiefen C. Inhibition of inflammatory lymphangiogenesis by integrin alpha5

blockade. Am J Pathol 2007;171:361-72.

30. Cursiefen C, Chen L, Saint-Geniez M, Hamrah P, Jin Y, Rashid S, Pytowski B, Persaud K, Wu Y, Streilein JW, Dana R. Nonvascular VEGF receptor 3 expression by corneal epithelium maintains avascularity and vision. Proc Natl Acad Sci U S A 2006;103:11405-10.

31. Anijeet DR, Zheng Y, Tey A, Hodson M, Sueke H, Kaye SB. Imaging and evaluation of corneal vascularization using fluorescein and indocyanine green angiography. Invest Ophthalmol Vis Sci 2012;53:650-8.

32. Zheng Y, Kaye AE, Boker A, Stewart RK, Tey A, Ahmad S, Willoughby CE, Bron AJ, Kaye SB. Marginal corneal vascular arcades. Invest Ophthalmol Vis Sci 2013;54:7470-7.

33. Yoon KC, Ahn KY, Lee SE, Kim KK, Im SK, Oh HJ, Jeong IY, Park SW, Park YG, Nah HJ, Im WB. Experimental inhibition of corneal neovascularization by photodynamic therapy with verteporfin. Curr Eye Res 2006;31:215-24.

34. Dastjerdi MH, Saban DR, Okanobo A, Nallasamy N, Sadrai Z, Chauhan SK, Hajrasouliha AR, Dana R. Effects of topical and subconjunctival bevacizumab in high-risk corneal transplant survival. Invest Ophthalmol Vis Sci 2010;51:2411-7.

35. Ang M, Sim DA, Keane PA, Sng CC, Egan CA, Tufail A, Wilkins MR. Optical Coherence Tomography Angiography for Anterior Segment Vasculature Imaging. Ophthalmology 2015;122:1740-7.

36. Yan M, Zhou J, Luo C, Xu T, Xing X. Multiscale Joint Optimization Strategy for Retinal Vascular Segmentation. Sensors (Basel) 2022;22:1258.

37. Myung D, Jais A, He L, Blumenkranz MS, Chang RT. 3D Printed Smartphone Indirect Lens Adapter for Rapid, High Quality Retinal Imaging. J Mob Technol Med 2014,3:9-15.

38. Sharma A, Subramaniam SD, Ramachandran KI, Lakshmikanthan C, Krishna S, Sundaramoorthy SK. Smartphone-based fundus camera device (MII Ret Cam) and technique with ability to image peripheral retina. Eur J Ophthalmol 2016;26:142-4.